SCIENCE CHINA
Earth Sciences

• RESEARCH PAPER •

May 2013 Vol.56 No.5: 806–817
doi: 10.1007/s11430-012-4578-x

# The plate contact geometry investigation based on earthquake source parameters at the Burma arc subduction zone

ZHANG LangPing[1], SHAO ZhiGang[1*], MA HongSheng[2], WANG XingZhou[3] & LI ZhiHai[4]

[1] *Key Laboratory of Earthquake Prediction, Institute of Earthquake Science, China Earthquake Administration, Beijing 100036, China;*
[2] *China Earthquake Administration, Beijing 100036, China;*
[3] *Earthquake Administration of Anhui Province, Hefei 230031, China;*
[4] *Earthquake Administration of Xinjiang Uygur Autonomous Region, Urumqi 830011, China*

Received September 29, 2012; accepted December 17, 2012; published online January 16, 2013

Accurately characterizing the three-dimensional geometric contacts between the crust of the Chinese mainland and adjacent regions is important for understanding the dynamics of this part of Asia from the viewpoint of global plate systems. In this paper, a method is introduced to investigate the geometric contacts between the Eurasian and Indian plates at the Burma arc subduction zone using earthquake source parameters based on the Slab1.0 model of Hayes et al. (2009, 2010). The distribution of earthquake focus depths positioned in 166 sections along the Burma Arc subduction zone boundary has been investigated. Linear plane fitting and curved surface fitting has been performed on each section. Three-dimensional geometric contacts and the extent of subduction are defined quantitatively. Finally, the focal depth distribution is outlined for six typical sections along the Burma arc subduction zone, combining focal mechanisms with background knowledge of geologic structure. Possible dynamic interaction patterns are presented and discussed. This paper provides an elementary method for studying the geometric contact of the Chinese mainland crust with adjacent plates and serves as a global reference for dynamic interactions between plates and related geodynamic investigations.

**Burma arc subduction zone, earthquake source parameters, plate boundary, geometric contact, Slab1.0 model**

**Citation:** Zhang L P, Shao Z G, Ma H S, et al. The plate contact geometry investigation based on earthquake source parameters at the Burma arc subduction zone. Science China: Earth Sciences, 2013, 56: 806–817, doi: 10.1007/s11430-012-4578-x

The study of continental crustal dynamics involves multiple disciplines that investigate lithospheric composition, structure, performance, dynamic evolution and deep driving mechanisms. This frontier field is a growing research area in the earth sciences during the 21st century [1, 2]. Some of the specific areas of interest are geophysical field effects, the intercontinental subduction of plates, plate margin tectonics, intraplate tectonics and block boundary investigations [3, 4]. The Chinese mainland is regarded as a dynamic system within the framework of global plate movements. The dynamic actions of the adjacent plates are the main source of exterior forces that affect its crustal motion. The Chinese mainland is a part of the Eurasian Plate that is bordered by the northwestern Pacific Plate, the Philippine Sea Plate and the Indian Plate [5]. The margins of these plates form the main zone of contact and interaction between the Chinese mainland and the exterior system [6]. Characterizing these geometric contacts and dynamic interactions is essential for understanding the lithospheric dynamics of the Chinese mainland.

The accumulation of crustal stress and strain within a

*Corresponding author (email: shaozg@seis.ac.cn)

crustal block is a typical mechanical process. Governing equations and definite conditions are usually used to describe such a mechanical problem. Governing equations include constitutive equations, kinematic equations and geometric equations, and the definite conditions consist of boundary and initial conditions. In the case of the Chinese mainland, geometric contacts and dynamic interactions between plates determine the boundary and exterior loading conditions as independent systems. This will provide essential references for dynamic investigations in the region, especially for multiply constrained numerical and physical simulations [4, 7].

Subduction zones are concentrated belts of earthquakes and magmatic activity [8, 9]. Contact patterns and dynamic interactions between plates at subduction zones have attracted much research in the past. In the 1970s, research began to describe the geometric contact between the Eurasian and Indian plates in the Himalayan arc region by considering the distribution of earthquake focuses combined with background geologic structure [10–15]. Investigations of the collisional process between the two plates focused on the dynamic interactions of the western and eastern Himalayan syntaxis, i.e., the Burmese arc subduction zone [16, 17] and the Hindukush-Pamir regions [18–21]. Using the characteristics of earthquake focus distributions, researchers described the geometric contact pattern between the of northwest Pacific Plate and the Eurasian Plate at the Japan Trench [22–26] and between the Philippine Sea Plate and Eurasian Plate at Taiwan [27, 28]. With the development of seismic tomography, researchers began to investigate northward subduction in the area north of the Himalayas, and in particular investigated the maximum range of Indian Plate subduction [29–36], in which the geometric contact between the plates was obtained by characterizing seismic velocity differences in the deep crust and upper mantle. Note that this method has also been used in the description of multiple contacts between plates around the world, especially in constraining the morphology of the subduction zones [37–42]. In addition, a global perspective on collisional processes between plates at subduction zones has been gained from the inversion of GPS observational data [43, 44], deep seismic reflection data [45–48] and other investigations [49, 50].

The Burma arc subduction zone, a typical zone of continental subduction, is the transformational region between the Himalayan collision belt and the Andaman arc [51, 52]. Santo [53] first noticed the oblique seismic zone beneath the Burma arc, and much subsequent research [10–12, 14–17, 54–61] has been undertaken to extend those observations. This has enabled the geometric characterization of the Indian Plate underthrusted into the Burma arc zone from west to east by choosing typical sections along the Burma arc. The development of this research has led to the discovery that although the subduction angle varies with depth [16, 60] it does not necessarily increase with depth [61]. In addition to describing the geometry of the Burma arc subduction zone based on earthquake source parameters, determinations of the velocity structure of the lithosphere beneath the Burma arc zone have been made using tomography [36, 39, 62, 63], which provides another way to constrain the nature of the geometric contact between the two major plates. Considering the spatial distribution characteristics of focal mechanism at this plate boundary, characterization of the stress field and the dynamic conditions of the subduction zone developed [16, 55–59, 64, 65]. It is generally acknowledged that the subduction zone was formed by the subduction and compression of the Indian Plate at the margin of the Eurasian Plate. The stress field of this zone directly reflects that the Indian Plate is underthrusted into the Burma arc zone from west to east.

Most of the above research has qualitatively described interaction patterns between plates using the distribution characteristics of earthquake focuses sometimes combined with tomographic images of velocity structure differences. Seismic dislocation between plates is a direct form of plate interaction. As the calibration accuracy of seismic parameters has improved over time [28, 66, 67], Hayes et al. [68–70] developed the Slab1.0 model using seismic parameters. This has enabled the quantitative development of a three-dimensional geometric model of plate-boundary patterns and dive ranges for subduction zones between several oceanic and continental plates.

In this paper we modify the model of the geometric contact between the Eurasian and Indian plates at Burma arc subduction zone, based on earthquake source parameters and referring to the Slab1.0 model of Hayes et al. [68, 69]. This results in the determination of a relatively well-constrained three-dimensional geometric pattern and dive range for the contact between the two plates. By combining this information with the spatial distribution characteristics of focal mechanism, the patterns of dynamic interaction between the two plates can be discussed.

## 1 Methods and procedure

### 1.1 Earthquake catalogs

The Burma arc is one of the most active earthquake regions on Earth, and it is also an area where continental intermediate-depth earthquakes are concentrated. The distribution of earthquake epicenters in the region is shown in Figure 1. This distribution is based on the historic earthquake catalog that originates from global Centroid Moment Tensor (gCMT) solutions of earthquakes with magnitudes above 5.5 (from 1976) maintained by Harvard University and the small earthquake catalog (from 1973) maintained by the US National Earthquake Information Center (NEIC). Using the ak135 travel-time model and seismic phase data, Engdahl et al. [66] redefined 138394 global events from 1964 to 2007 and compiled the corresponding earthquake catalog, which

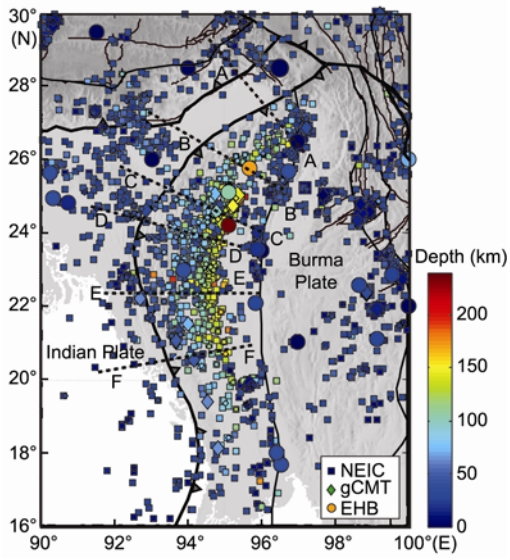


**Figure 1** Distribution of the epicenters and the focal depths of earthquakes at the Burma Arc subduction zone. The thick black solid lines denote the boundary of primary blocks, and the black triangles show the plate underthrust direction. The black lines express the boundary of secondary blocks [71]. The dotted lines denote six sections intercepted by the literature [63]. Different focal depths are labeled by different colors. The circles denote the EHB and Engdahl catalogs [66, 67] (http://www.isc.ac.uk/EHB/). The diamonds denote the Global Centroid Moment Tensor catalog (http://www.globalcmt.org/CMTsearch.html). The squares represent the National Earthquake Information Center catalog (http://earthquake.usgs.gov/regional/neic/).

apparently improved the precision of spatial seismic locations. To supplement the record with earthquake events prior to 1964, Engdahl and Villasefior [67] assembled a catalog of earthquakes with magnitudes over 7.0 from 1900 to 1999. From the distribution of the focal depth in Figure 1, it can be seen that the intermediate shocks are distributed along an area of the subduction zone from 19°N to 27°N with the maximum depth > 200 km. The distribution of focal depths in the region of interest roughly corresponds to the outlined region where the Indian Plate is underthrusted from west to east into the Burma arc zone.

### 1.2 Selection of earthquake events

First, a point at the boundary of the block is set as the reference point. Then, the line tangent to the block boundary at the reference point and the normal line perpendicular to this line and pointing in the direction of subduction are determined. Several equidistant nodes are selected along the normal line (20 km is used in this paper). Taking the reference point as the starting point and the normal as the central axis, a rectangular region is determined on the subduction side of the plate boundary; this is indicated in Figure 2(b) as the light blue region. The width of this rectangular region is 200 km, i.e., this region is defined such that the distance to the central axis is not greater than 100 km. The length of this rectangular region is the maximum distance from the spatial focal distribution to the tangent line.

To eliminate the influence of shallow earthquakes and the earthquakes below the reference point on the morphology of plate subduction zone, the angle between the horizontal plane and the plane formed by the epicentral point and the tangent line at the reference point is limited to the range of 5° to 60° [68, 69], i.e., the yellow triangular prism shown in Figure 2(c) determines the effective spatial range that is used to select the earthquake events, and it serves as a filter for the earthquake catalog. Earthquake events from outside this region are not included in the calculation. Taking the section shown in Figure 2(d) as an example, the horizontal normal line at the reference point is set as the horizontal axis, and the depth direction is defined as the vertical axis. All events with epicentral distances $\leqslant$100 km are projected to the section. The epicenters with color labels in Figure 2(d) denote earthquake events covered in the area represented by the yellow triangular prism shown in Figure 2(c). The epicenters labeled in grey represent earthquake events from outside the effective region.

Using the yellow region in Figure 2(c) as a filter, the EHB, NEIC and gCMT catalogs were selected. Earthquakes within this region constitute the effective catalog, which is used to investigate the contact condition of blocks at this reference point. There is an overlap between earthquakes selected by the three catalogs. To guarantee the credibility of depth fitting, the overlapping earthquakes need to be removed. The epicenter of each earthquake can only participate in one calculation. According to academic experience, the spatial precision of earthquake locations in the EHB, NEIC, and gCMT catalogs decreases in turn [66, 68]. Therefore, for the same earthquake event, if the EHB catalog is available, it is used preferentially. Positions from the NEIC catalog come next, and the gCMT catalog comes last. In the actual calculation process, due to the fact that both the time range and the lower limit of earthquake magnitude from the NEIC catalog cover those of the gCMT catalog, all earthquake events recorded by gCMT are also recorded by the NEIC catalog. Therefore, the gCMT catalog is not used for its positional information on the centers of seismic moments. In this paper, only the EHB and NEIC catalogs are needed for the discussion of the distribution of focal depths. Considering that the minimum magnitude event in the EHB catalog is $M_b$4.7 [66], seismic source parameters provided by the EHB catalog are used for all events from 1900 to 1973 and for those from 1973 to 2007 with magnitudes $\geqslant$5.0. The seismic source parameters from the NEIC catalog are used for events from 1973 to 2007 with magnitudes < 5.0 and for all events after 2007.

### 1.3 Linear planar fitting of the plate interface

Due to the influence of positioning accuracy, seismic hypocenters recorded in earthquake catalogs have some degree of uncertainty, and generally, these errors in spatial location

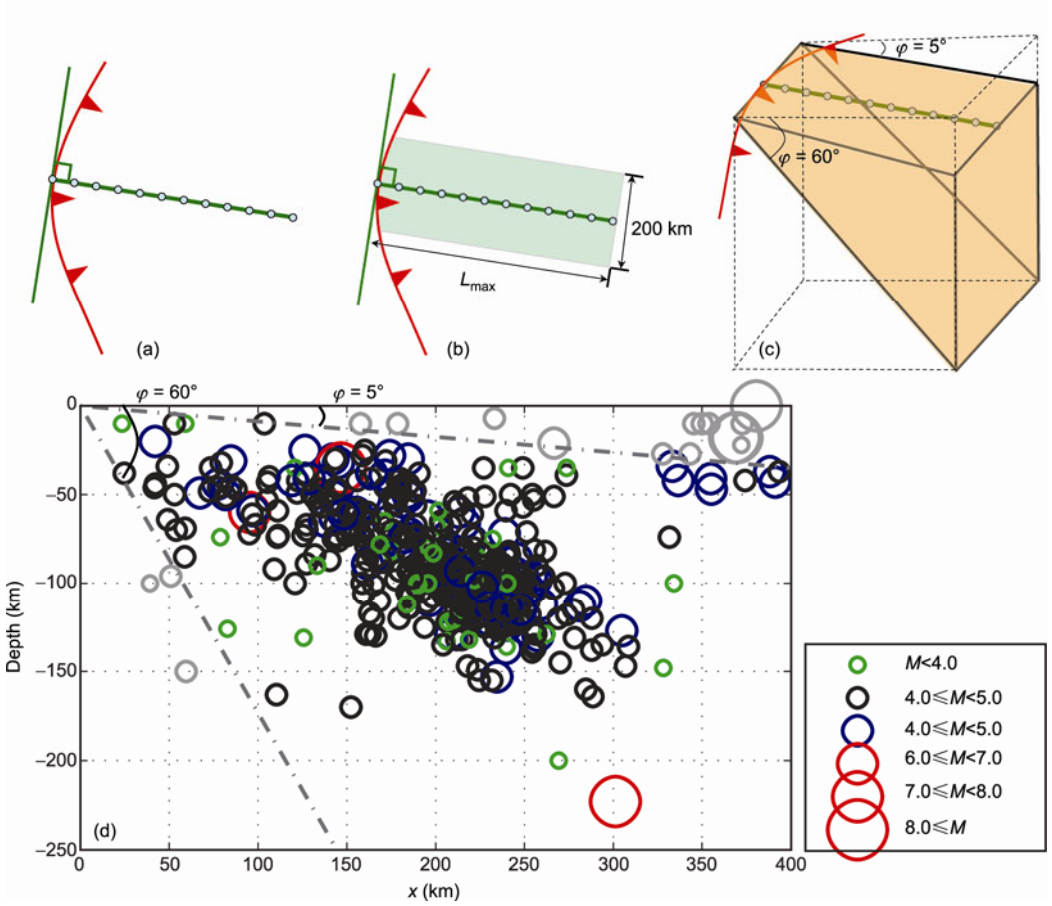


**Figure 2** Process of earthquake catalog selection. (a) Select a point at the boundary of a subduction block, the normal of the boundary is set as the central line of the section. Equidistant nodes are selected along this central line. (b) A rectangular region is selected along the central axis with a width of 200 km and a length of $L_{max}$. $L_{max}$ is determined by earthquake distribution characteristics. (c) The yellow triangular prism formed by two planes with direction angles to the horizontal plane of 5° and 60° determines the effective spatial extent that is used to select the earthquake events, i.e., this region is a filter of the earthquake catalog. (d) Taking an actual section as an example, the color labeled epicenters denote earthquake events passing through the earthquake catalog filter, and the grey labeled epicenters represent earthquake events outside the earthquake catalog filter.

are expected to have a normal distribution. However, in comparison with the scale of plate boundaries and the error in focal depth, horizontal errors in epicenter positions are much smaller. Therefore, the horizontal locations are assumed to be known and fixed, whereas focal depths are uncertain and determined by a probability density function. This probability density function is a normal function with expectancy determined by the focal depth given by relevant organizations. The difference between the actual focal depth of an earthquake and that given by relevant organizations is calculated with standard errors. Parameters of focal depth are provided in both EHB and NEIC catalogs. Standard errors of focal depths are available in the EHB catalog. For the NEIC catalog, the standard error of the focal depth is regarded as a constant. In this paper, this standard error used is ±18 km [68]. Additionally, earthquake events with different magnitudes are assigned different weighted coefficients. The larger the magnitude of the earthquake is, the higher the weighted coefficient is, which is consistent with the scale of fracturing in actual earthquakes [72].

After selecting and filtering an earthquake catalog, the epicenters of effective earthquakes are projected to a section through the reference point. The angle of the subduction plane between plates is calculated according to the distribution of focal depths in the section. Assuming that the subduction angle $\delta$ varies from 5° to 60°, the maximum likelihood method can be used to determine the subduction angle expressed as

$$P(\delta)=\prod_{i=1}^{i=n}\left\{\left[\frac{1}{\sigma_i\sqrt{2\pi}}\exp\left\{-\frac{[x_i(\delta)-\mu_i]^2}{2\sigma_i^2}\right\}\right]\omega_i+\omega\right\}, \quad (1)$$

where $\sigma_i$ denotes the variance of the probability density function followed by the depths of earthquake events, $x_i(\delta)$ represents the theoretical focal depth calculated according to the inclination of the subduction plane and the transverse distance to the plate boundary, $\mu_i$ represents the expectation of the probability density function (which is set as the reported focal depth), $\omega_i$ is the weighted coefficient of an earthquake event (the value of which is related to the square of the earthquake magnitude), and $\omega$ is a parameter

used to avoid problems that arise if the first term within the brackets is close to zero (usually set as 0.1). By a logarithmic transformation of eq. (1), the product form is transformed to the sum form and expressed as:

$$P'(\delta)=\sum_{i=1}^{i=n}\log\left\{\left[\frac{1}{\sigma_i\sqrt{2\pi}}\exp\left\{-\frac{[x_i(\delta)-\mu_i]^2}{2\sigma_i^2}\right\}\right]\omega_i+\omega\right\}. \quad (2)$$

Taking the reference point in Figure 3(a) as an example, first, the normal line of the plate boundary at the reference point are determined. Then, the earthquake catalog is filtered to select earthquake events satisfying the prescribed conditions. The red box in Figure 3(a) denotes the spatial position of the filter. The colored epicenters in Figure 3(a) represent the earthquake events with distribution characteristics that satisfy the selection rule. These epicenters are

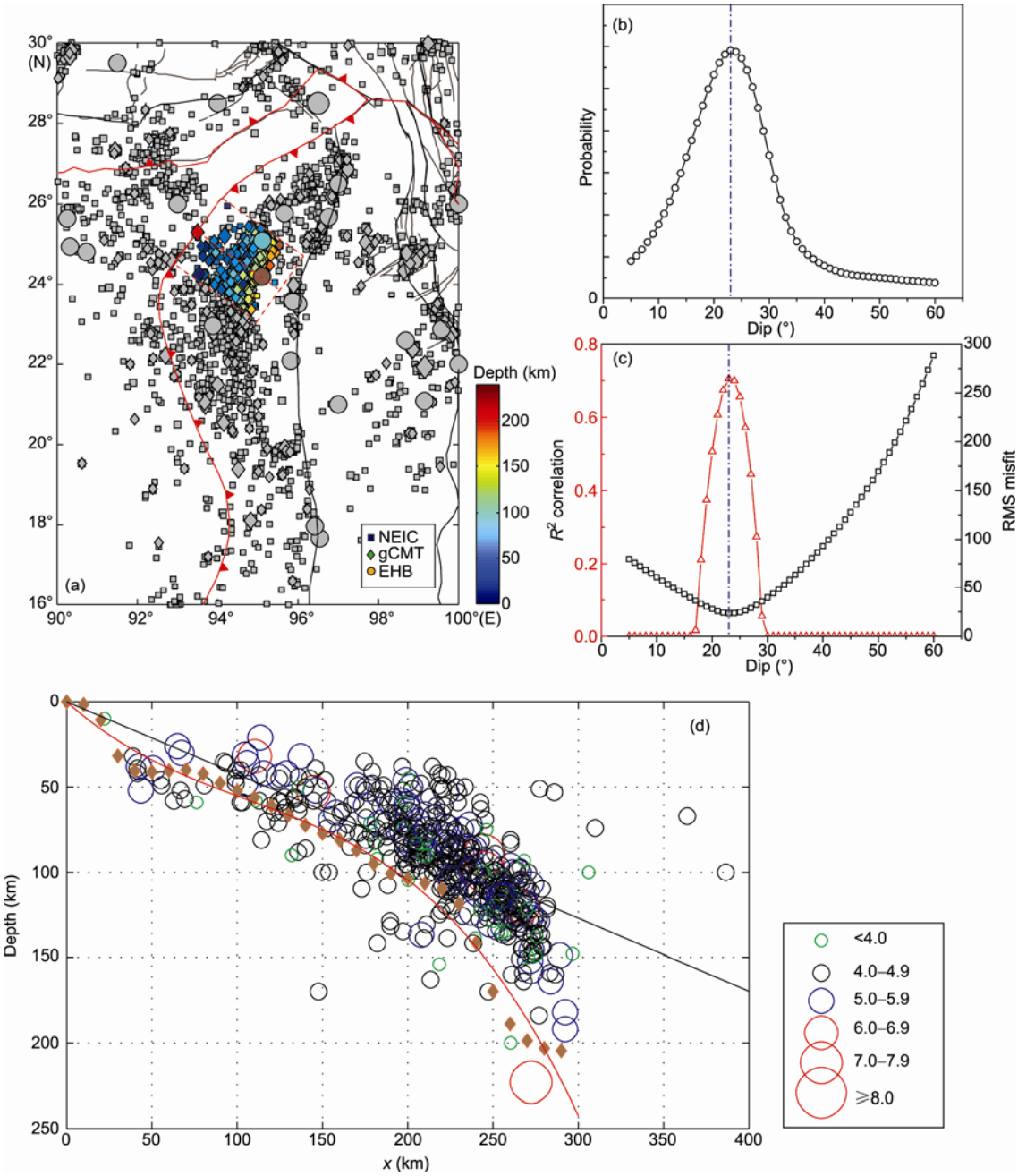


**Figure 3** Projection of focal depth in a classical section. (a) Spatial location of the section and the project distribution of epicenters of earthquakes satisfying the selection condition. The red dashed line represents the spatial range of this section, the grey marked events denotes the epicenter distribution of the research region, the colored events correspond to the epicenter distribution of the earthquakes that satisfy the catalog filter, and the red diamond corresponds to the location of the reference point. (b) The relational curve between the probability value and the inclination by linear plane fitting; inclination varies from 5° to 60°. (c) The relationship between the linear fitness of the focal depth, residual and the inclination. (d) The projection of the focal depth and the fitting results, where the black line denotes the linear plane fitting results, the inclination with the horizontal axis is the inclination of the subduction plane at this reference point, the red diamonds represent the characteristic depth at the uniform nodes at the axis, the red solid line corresponds to the nonlinear surface fitting results of red diamonds and reflects the plate contact condition at the reference point.

projected to a section. The reference point is set as the origin on the section, with the central axis corresponding to the horizontal axis, and the depth direction defined as the vertical axis, as shown in Figure 3(d). The inclination $\delta$ at this reference point varies from 5° to 60°, with slips at an interval of $\Delta\delta$=1°. Using eq. (2) to calculate $P'(\delta)$, a relational curve between $P'(\delta)$ and the inclination is shown in Figure 3(b). When the inclination is 23°, $P'(\delta)$ was found to reach its maximum value. Therefore, the subduction angle for this reference point is taken to be 23°, i.e., the contact pattern between plates is a plane with an inclination of 23°.

To verify the credibility of the linear plane fitting, the fitting results are analyzed through residual analysis and fitting relevance analysis. The residual can be expressed as

$$RMS(\delta)=\frac{\sum_{i=1}^{i=n}\omega_i(\mu_i-x_i(\delta))^2}{\sum_{i=1}^{i=n}\omega_i}, \tag{3}$$

where $RMS(\delta)$ represents the fitting residual corresponding to the inclination of $\delta$. The fitting relevance can be expressed as

$$R^2=1.0-\frac{\sum_{i=1}^{i=n}\omega_i(\mu_i-x_i(\delta))^2}{\sum_{i=1}^{i=n}\omega_i(\mu_i-\overline{\mu})^2}, \tag{4}$$

where $R$ is the fitness and $\overline{\mu}$ denotes the average focal depth. The residual and fitness are usually used to evaluate the quality of fitting results. The lower the residual is, or the higher the fitness is, the better the fitting result is. The fitting results of residual and fitness, based on the focal depth, are shown in Figure 3(c). When the inclination is 23°, the residual and fitness reach minimum and maximum values, respectively. Moreover, the fitness exceeds 0.7, which indicates that linear plane fitting results are credible.

### 1.4 Nonlinear surface fitting of a plate contact

The linear plane fitting result is shown in Figure 3(d) as a black solid line. The orientation of this line relative to the vertical axis corresponds to the subduction angle at this reference point. The linear plane fitting results reveal, to some extent, the nature of the subducting plates. However, subduction angles are not expected to be constant, which means that a subduction contact would be better described as a surface rather than as a plane. Previous research has confirmed that subduction angle should vary with depth. Therefore, nonlinear surface fitting is necessary, as will be illustrated in detail in this section.

First, based on the distribution characteristics of focal depths, it can be seen that the filtered earthquake catalog still may contain shallow earthquakes. For example, several earthquakes in Figure 3(d) with a vertical axis between 300 and 400 km have a depth between 50 and 100 km, which makes them apparent shallow earthquakes. Therefore, before nonlinear surface fitting, the shallow earthquakes from the filtered earthquake catalog should be eliminated. Based on the subduction angle and distribution characteristics of focal depth determined by linear plane fitting, the range of the inclination is modified in this paper. The minimum value of inclination $\delta_{\min}$ used by the earthquake catalog filter varies with the vertical axis, and it is expressed as

$$\delta_{\min}=\begin{cases}5^\circ, & x<150\text{ km},\\ (5+(x-150)/20)^\circ, & x\geqslant 150\text{ km},\end{cases} \tag{5}$$

where $\delta_{\min}$ is the lower limit of the inclination range. When the lateral distance to the plate boundary exceeds 150 km, the lower limit of inclination varies with distance to the plate boundary.

Nonlinear surface fitting is then performed for the remaining earthquakes after eliminating shallow earthquakes. For the purpose of nonlinear surface fitting, the focal depths of earthquake events are concentrated to uniform nodes along the central axis of the section. Then, the characteristic depth at each uniform node, representing the depth distribution of the section, is used to perform nonlinear surface fitting. The characteristic depth at each uniform node is calculated by

$$Z(x)=\frac{\sum_{i=1}^{i=n}\Omega_i(M_i,x_i)\mu_i}{\sum_{i=1}^{i=n}\Omega_i(M_i,x_i)}, \tag{6}$$

where $Z(x)$ denotes the characteristic depth of the node, and $x$ is the horizontal ordinate of the node. $\Omega_i(M_i,x_i)$ represents the influence coefficient of the magnitude and spatial location of the $i$th earthquake event. $M_i$ is the magnitude of the $i$th earthquake event, and $\mu_i$ is its focal depth. Considering the relationship between the magnitude and the rupture area, and the attenuation rule for earthquake wave energy, the weighted coefficient can be calculated by

$$\Omega_i(M_i,x_i)=10^{M_i}\exp\left(-\frac{(x-x_i)^2}{2D}\right), \tag{7}$$

where $D$ is a parameter that adjusts the weighted coefficient of the spatial location (200 km$^2$ in this paper). The first term in eq. (7) is seen to reflect the influence of magnitude on the weighted coefficient, whereas the second term corresponds to the influence of the lateral distance to the node on the weighted coefficient.

The characteristic depths of nodes along the central axis are calculated, in turn, until there are no cataloged earth-

quakes left on the positive side of the $x$ axis, as shown by the red diamond in Figure 3(d). Prior to fitting the characteristic depths of nodes, and considering that the node at $x$=0 (i.e., the reference point) is a point on the boundary, the depth at this point can be set to zero. Therefore, the constant term of the polynomial expression is zero. Ref. [69] points out that polynomial expression fitting can easily lead to irrational oscillation bending and instead suggests second to fourth order polynomial expression fitting. The third order polynomial expression fitting result is shown as the red line in Figure 3(d).

### 1.5 Plate contact fitting at the Burma arc subduction zone

Using to the above method, 166 sections from south to north along the Burma arc subduction zone were selected for nonlinear surface fitting. The fitting results for each section produced a three-dimensional geometric contact surface in Figure 4(b) with depths denoted by colors. The results show that the Indian Plate apparently underthrusted from west to east into the Burma arc subduction zone. The maximum subduction depth occurs around 24°N. Moreover, there is a semicircular zone of concentrated depths here which reveals that the subduction from west to east dominates the contact surface at 24°N. This transitions to NW-SE subduction in the north and SW-NE subduction in the south. This is consistent with the results of previous research [11, 63]. During the process of nonlinear surface fitting, if there are no earthquakes found at the appropriate depth and direction at the nodes of the central axis, the calculation stops. Therefore, the boundary line marking the edge of the colored region in Figure 4(b) corresponds to the locked line of two large plates [73], i.e., the maximum contact region where earthquake rupture is the main reflection pattern. Moreover, most of the locked line is located to the west of 96°E, whereas only the section north of 24°N exceeds 96°E.

## 2 Results and discussion

The Slab1.0 model proposed by Hayes et al. [68–70], has been modified in this paper and applied to the three-dimensional geometric contact between the Eurasian and Indian plates at the Burma arc subduction zone. Taking the points on the plate boundary as reference points, sections were selected, and earthquake catalog filtering was established. With regard to the distribution characteristics of focal depths, linear plane fitting and nonlinear surface fitting were performed to constrain the plate contact pattern at the reference points. 166 sections were selected along the Burma arc subduction zone. Considering the nonlinear surface fitting of focal depths at each of the sections, the three-dimensional geometric configuration of the Indian Plate was underthrust eastward in the vicinity of the Burma arc; the location of the locked part of the line between the two large plates was given quantitatively and more accurately.

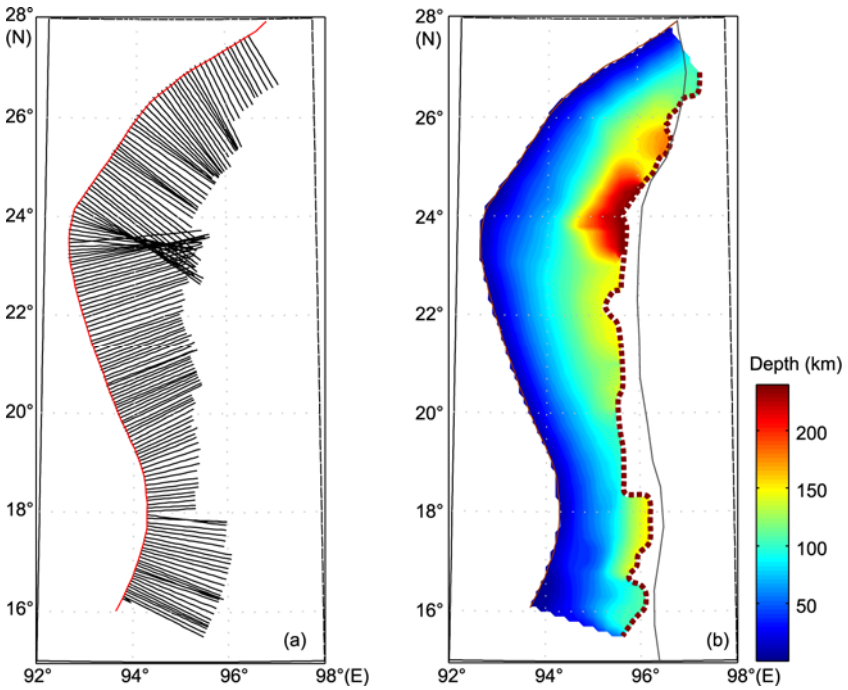


**Figure 4** Selection of sections in the Burma Arc subduction zone and nonlinear spatial fitting results. (a) The spatial location of sections selected in Burma Arc subduction zone. (b) 3D geometric contact between the Indian plate which subducted eastward at the Burma Arc subduction zone and the Burma Plate, the locked line of plate contact is represented by red dashed line, the red solid line denotes the plate boundary and the grey solid line corresponds to the Sagaing rupture.

During the linear plane fitting process that was applied to several sections across the Burma arc subduction zone, the removal of shallow earthquakes was necessary to avoid their influence on the linear plane fitting results. The inclusion of shallow earthquakes in the analysis would lead to an underestimation of the inclination of the subduction plane; this is why they need to be filtered out. In the paper, the method of Hayes and Wald [68] is used for reference. Earthquake events with inclinations <5° are removed to guarantee that shallow earthquakes within a certain distance of the section will not be included in the calculation of inclination. Earthquake events with an inclination of >60° are also removed, based on previous research that found that inclinations in the Burma arc subduction zone do not exceed 60°. As in the case of linear plane fitting, shallow earthquakes also influence nonlinear surface fitting results to a certain extent. The eastern side of the Burma arc subduction zone is dominated by Sagaing rupture and there are many shallow earthquakes in the vicinity of this rupture zone. Therefore, before nonlinear surface fitting, the inclination of the subduction surface is obtained by linear plane fitting and earthquakes with a horizontal ordinate over 150 km and above the inclination of the subduction plane are regarded as shallow earthquakes and removed from the catalog. This three-dimensional geometric analysis process enables the manual removal of shallow earthquakes [61], thereby automatically removing their influence.

In previous geometric studies of the contact between plates, most of research has involved sections that are selected along a plate boundary to investigate the distribution of focal depth characteristics. Based on earthquake source parameters, Hayes et al. [68–70] developed the Slab1.0 model to study the three-dimensional geometry of plate boundaries. Using this method, several subduction zones with relatively simple subduction patterns have been analyzed. This has led to more quantitative results and more accurate geometric contact information. However, the boundary between the Indian and Eurasian plates defined by Bird [74], and used in that paper, involves the Sagaing rupture, which means that the Slab1.0 model is not suitable for the Burma arc subduction zone. If a study were developed for Sagaing rupture using the Slab1.0 model, a contradictory conclusion would be obtained. Therefore, this work with the Burma arc subduction zone not only characterizes the contact conditions between the Chinese mainland and its adjacent plates, but also complements previous studies.

The three-dimensional geometric configuration of the boundary between the Indian and Eurasian plates at the Burma arc subduction zone is given in Figure 4(b). This is a static description of the contact between two large plates, and dynamic interaction between the two plates is not involved. The interaction between these two big plates at the Burma arc subduction zone is investigated through the distribution of focal-depth characteristics along six typical sections indicated by black dashed lines in Figure 1. The positions, central point ordinates, and projection range of vertical sections are shown in Table 1. Using focal mechanism solutions provided by the gCMT catalog, the focal mechanisms of earthquake events in the projection range are projected to each section as shown in Figure 5. The relative latitudinal distance to the point (at 18°N, 90°E) is set as the horizontal axis. Statistical results for the focal mechanism determined for each section are listed in Table 1. The horizontal ordinates of the epicenters of intermediate earthquake events along the six sections are mostly less than 600 km, which is consistent with the observation that most of the locked line in Figure 4(b) does not exceed 96°E. However, 96°E corresponds to the spatial location of the Sagaing rupture, shown by a blue triangle in Figure 5. From the distribution characteristics of focal mechanism solutions for each section, a large number of shallow strike-slip earthquakes are seen to exist coincident with the position of Sagaing rupture, which is in agreement with the right-lateral strike-slip mechanism for the Sagaing rupture. In addition, at a position with a horizontal ordinate of about 800 km, two sections A-A′ and B-B′ show indications of both normal fault and strike-slip earthquakes. This corresponds to the fault characteristics of strike-slip and the extension of the Tengchong-Longling seismic zone in the Yunnan-Burma block [75].

Figure 5 shows that the focal mechanisms of sections B-B′, C-C′, D-D′ and E-E′ can be possibly divided into two segments at a horizontal ordinate of 400 km. Strike-slip earthquakes dominate the western sector, but a small number of subduction earthquakes occur. This demonstrates that the interaction between blocks in this region is dominated by strike-slip motion and that only a few thrust earthquakes with small subduction angles exist. In contrast, the eastern

**Table 1** The positions, thicknesses, strike angles and focal mechanism of six sections in Burma Arc subduction zone

| ID | Central ordinate | | Strike angle | Projection range | Pattern of focal mechanism | | | |
|---|---|---|---|---|---|---|---|---|
| | Latitude (N) | Longitude (E) | (°) | (km) | Normal fault | Subduction | Strike-slip | Total |
| A-A′ | 27.788° | 95.827° | 140 | ±100 | 3 | 9 | 12 | 24 |
| B-B′ | 26.284° | 94.717° | 120 | ±70 | 9 | 9 | 21 | 39 |
| C-C′ | 25.270° | 93.380° | 115 | ±70 | 0 | 22 | 19 | 41 |
| D-D′ | 24.180° | 93.490° | 105 | ±100 | 2 | 21 | 23 | 46 |
| E-E′ | 22.380° | 93.410° | 90 | ±100 | 3 | 11 | 13 | 27 |
| F-F′ | 20.600° | 93.660° | 80 | ±100 | 7 | 2 | 7 | 16 |

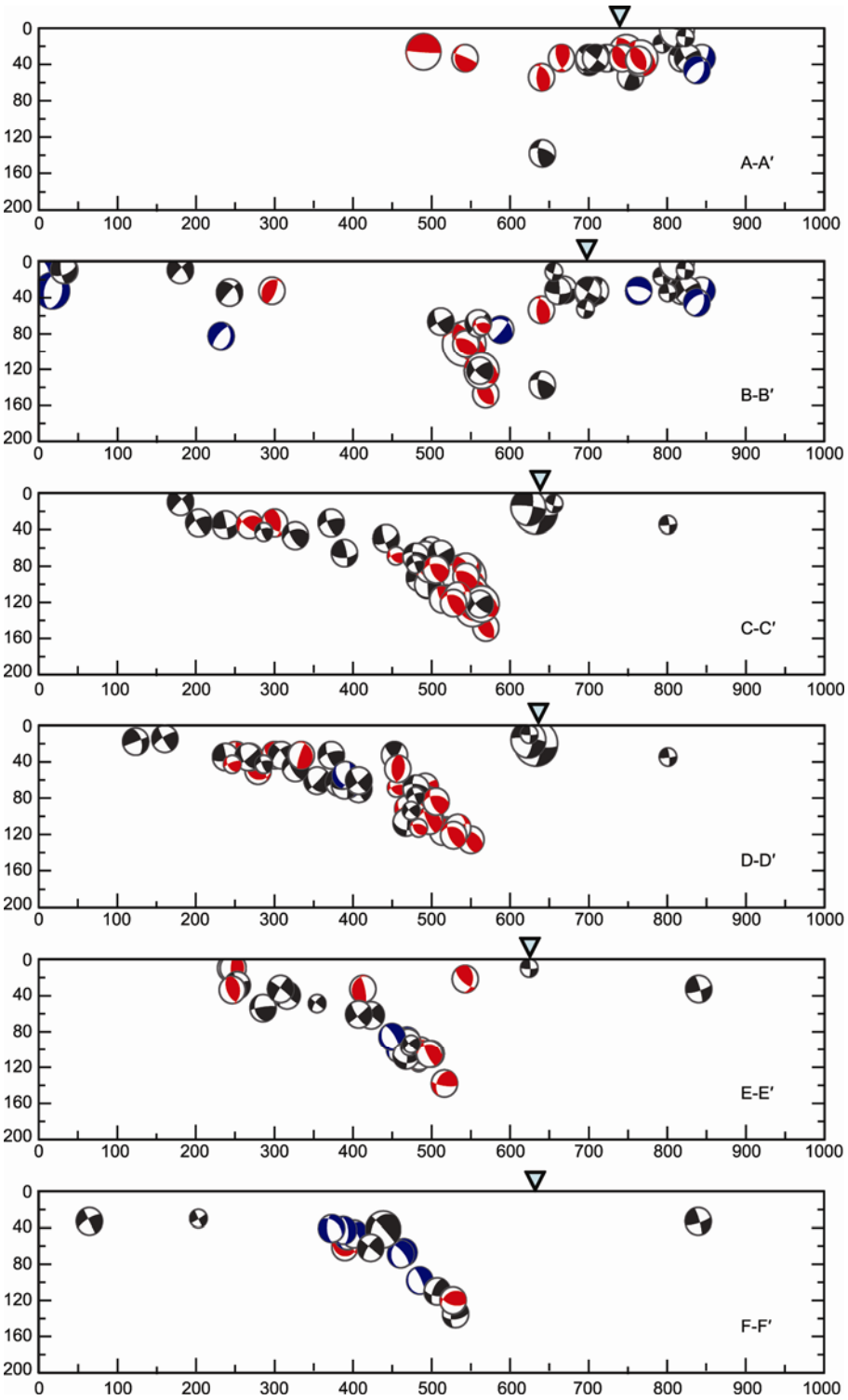


**Figure 5** Distribution of focal depth and focal mechanism solutions for six typical sections in the Burma Arc subduction zone. The spatial positions of the six sections are shown in Figure 1. The projection range for earthquakes was set by that of the distances from the central line of the section. These are 100, 70, 70, 100, 100, and 100 km respectively, where the vertical axis denotes focal depth, and the horizontal axis represents the relative latitudinal distance to the reference point (18°N, 90°E). The blue focal mechanism solutions represent normal fault earthquakes, the red ones denote subduction earthquakes, and the black ones represent strike-slip earthquakes. The light blue triangles represent the position of Sagaing ruptures in this section. The focal mechanism solutions originate from seismic moment tensor solutions of earthquakes with magnitudes above 5.5 from 1976 given by Harvard University (the gCMT catalog).

section is thrust oriented, and a small number of strike-slip earthquakes have occurred here. The thrust domination of the eastern section indicates that the subduction angle is large. This is consistent with the results showing concentrated gradient contours at 24°N, as shown in Figure 4(b). The region with a lower gradient contour is thrust oriented,

whereas the region with a higher gradient contour is strike-slip oriented. It can be seen from the distribution characteristics of the focal mechanism of these four sections that a semicircular region with a high gradient contour at 24°N in Figure 4(b) exerts strong thrust characteristics. Therefore, the geometric contact results of this region have been verified from the perspective of the distribution characteristics of focal mechanisms. Combining the three-dimensional geometric contact in Figure 4(b) with the distribution characteristics of a focal mechanism in Figure 5, the dynamic interaction between two large blocks is observed to be W-E thrust oriented at 24°N. This gradually transforms to a NW-SE oriented thrust in a northward direction, and to a SW-NE thrust in a southward direction.

The motion and dynamic patterns of the Burma arc subduction zone, lying between two large plates, have always attracted the attention of geodesy. In recent years, the study of this problem was progressed rapidly. Combining seismic data collection activities with analyses of velocity structure enabled Hu et al. [63] to point out that the Indian Plate began underthrusting around 94°E and converged at the position of the Sagaing rupture. Using a block model, Meade [76] simulated and analyzed the current patterns of motion in the Indian-Eurasian plate collision region, and concluded that subduction and strike-slip are the main motion patterns seen in the Burma arc subduction zone. It was also revealed that the Burma arc underthrusted from west to east as it moved in a NNE direction. Using geodetic data, slip rates of geologic faults and the regional tectonic stress field (earthquake moment tensors), attempts were made to try to establish the dynamic pattern of the crust southeast of the Qinghai-Xizang Plateau [77–80]. Results of this work qualitatively constrained the three-dimensional geometric contact pattern between the two large blocks of the Burma arc subduction zone. However, this paper, based directly on seismic data was able to quantitatively and more accurately characterize the boundary. These results constitute an essential reference for future work.

In this paper, a generalized method based on earthquake source parameters used to constrain three-dimensional geometric contacts between lithospheric blocks was proposed and applied to the Burma arc subduction zone between the Asian and Indian plates. This subduction belt has a relatively simple underthrust pattern, and is one of several plates bordering China (cf., the northwest Pacific and Philippine Sea plates). However, establishing the static interaction between the Chinese mainland and its adjacent plates still needs further research. In addition, this paper has been limited to static interactions between blocks. Dynamic block interactions, the magnitude and direction of interactional forces, and the patterns of interactions of plates beneath the locked line still need further work involving focal mechanism solutions and the analysis of observational geophysical field data.

*The authors thank Prof. Liu Guiping in the China Earthquake Administration for the good guidance and discussion, and the anonymous reviewers for offering constructive advice and useful guidance. This work was supported by the National Science and Technology Support Plan Project (Grant No. 2012BAK19B01-04).*

1 Xu Z Q, Yang J S, Ji S C, et al. On the continental tectonics and dynamics of China (in Chinese). Acta Geol Sin, 2010, 84: 1–29
2 Xu Z Q, Li T D, Yang J S, et al. Advances and prospectives of continental dynamics: Theory and application (in Chinese). Acta Petrol Sin, 2008, 24: 1433–1444
3 Teng J W, Bai W M, Zhang Z J, et al. Development direction and ponders of the Continental dynamics in China (in Chinese). Prog Geophy, 2009, 24: 1913–1936, doi: 10.3969/j.issn.2004-2903.2009.06.001
4 Teng J W. The developmental opportunity and challenge of geophysics in the present age in China (in Chinese). Prog Geophy, 2007, 22: 1101–1112
5 Zhang G M, Li X Z, Geng L M. Seismic activity along the northern boundary of India plate and earthquake in China's continent (in Chinese). Earthquake, 1994, 14: 1–9
6 Fu Z X, Jiang L X. On large-scale spatial heterogeneities of great shallow earthquakes and the plates coupling mechanism in Chinese mainland and its adjacent area (in Chinese). Earthq Res China, 1997, 13: 1–9
7 Liu Q Y, Wu J C. On numerical forecast of earthquakes—Thinking about the strategy for promoting earthquake prediction (in Chinese). Earth Sci Front, 2003, 10(Suppl): 217–224
8 Hacker B R, Peacock S M, Abers G A, et al. Subduction factory: 2. Are intermediate-depth earthquakes in subducting slabs linked to metamorphic dehydration reactions? J Geophys Res, 2003, 108(B1), doi: 101029/2001JB001129
9 Peacock D C. Scaling of transfer zones in the British Isles. J Struct Geol, 2003, 25: 1561–1567
10 Shi Z L, Huan W L, Wu H Y, et al. On the intensive seismic activity in China and its relation to plate tectonics (in Chinese). Sci Geol Sin, 1973, 4: 281–292
11 Shi Z L, Huan W L, Wu H Y, et al. On the intensive seismic activity in China and relation to plate tectonics. Am J Sci, 1975, 275-A: 239–259
12 Ye H, Liang Y S, Shen L Q, et al. The analysis of the recent tectonic stress of the Himalaya Mountains arc and its vicinities (in Chinese). Sci Geol Sin, 1975, 1: 32–49
13 Huan W L, Wang S Y, Shi Z L, et al. The distribution of earthquakes foci and plate motion in the Qinghai-Xizang Plateau (in Chinese). Chin J Geophys, 1980, 23: 269–280
14 Teng J W, Wang S Z, Yao Z X, et al. Characteristics of the geophysical fields and plate tectonics of the Qinghai-Xizang Plateau and its neighbouring regions (in Chinese). Chin J Geophys, 1980, 23: 269–280
15 Teng J W, Wei S Y, Sun K Z, et al. The characteristics of the seismic activity in the Qinghai-Xizang (Tibet) Plateau of China. Tectonophysics, 1987, 134: 129–144
16 Zhang J, Zang S X. Characteristics of earthquakes distribution and the mechanism of earthquakes in the boundary area between Burma, India and China (in Chinese). Acta Seismol Sin, 1986, 8: 240–253
17 Zang S X. The characteristics of the subduction zone beneath the Burmese arc and its stress state (in Chinese). Acta Seismol Sin, 1987, 2: 144–158
18 Chatelain J L, Roecker S W, Hatzfeld D, et al. Microearthquake seismicity and fault plane solutions in the HinduKush region and their tectonic implications. J Geophys Res, 1980, 85: 1365–1387
19 Ning J Y, Zang S X. The distribution of earthquakes and stress state in Pamir-Hindukush regions (in Chinese). Acta Geophys Sin, 1990, 33: 657–669
20 Fan G, Ni J F, Wallace T C. Active tectonics of the Pamirs and Karakorum. J Geophys Res, 1994, 99: 7131–7160
21 Sun W B, He Y S, Chang Z, et al. The plate subduction and stress state in the Pamir-Hindu Kush region (in Chinese). Seism Geol, 2009,

31: 207–217
22 Sun W B, He Y S, Li Y B. Subduction of the Pacific plate in the sea of Japan and earthquake of Northeastern China (in Chinese). Acta Seismol Sin, 1985, 7: 33–44
23 Ning J Y, Zang S X. The distribution of earthquakes and stress state in the Japan sea and the Northeast China (in Chinese). Seism Geol, 1987, 9: 49–61
24 Zang S X, Ning J Y. Study on the subduction in western Pacific and its implication for the geodynamics (in Chinese). Acta Geophys Sin, 1996, 39: 188–202
25 Sun W B, He Y S. Characteristics of the subduction zone in the western Pacific and its stress state (in Chinese). Chin J Geophys, 2004, 47: 433–440
26 Sun W B, He Y S. The feature of seismicity in northeast China and its relation to the subduction of the Japan sea plate (in Chinese). Seism Geol, 2004, 26: 122–132
27 Lacombe O, Mouthereau F, Angelier J, et al. Structural, geodetic and seismological evidence for tectonic escape in SW Taiwan. Tectonophysics, 2001, 333: 323–345
28 Wu Y M, Chang C H, Zhao L, et al. A comprehensive relocation of earthquakes in Taiwan from 1991 to 2005. Bull Seismol Soc Amer, 2008, 98: 1471–1481
29 Lü Q T, Jiang M, Xu Z Q, et al. Tomography evidence for India plate underthrusting only beneath Tethyan Himalaya (in Chinese). Chin Sci Bull, 1998, 43: 1308–1311
30 Zhou H W, Murphy M A, Lin Q L. Tomographic imaging of the Tibet and surrounding region: Evidence for wholesale underthrusting of Indian slab beneath the plateau (in Chinese). Earth Sci Front, 2002, 9: 285–292
31 Tilmann F, Ni J, INDEPTH Seismic Team. Seismic imaging of the downwelling Indian lithosphere beneath central Tibet. Science, 2003, 300: 1424–1427
32 Xue G Q, Su H P, Qian H, et al. Seismic tomographic constrain on the northward of the India plate. Acta Geol Sin, 2006, 80: 1156–1160
33 Zheng H W, Li T D, Gao R, et al. Teleseismic P-wave tomography evidence for the Indian lithospheric mantle subducting northward beneath the Qiangtang terrane (in Chinese). Chin J Geophys, 2007, 50: 1418–1426
34 Oreshin S, Kiselev S, Vinnik L, et al. Crust and mantle beneath western Himalaya, Ladakh and western Tibet from integrated seismic data. Earth Planet Sci Lett, 2008, 271: 75–87
35 Negredo A M, Replumaz A, Villaseñor A, et al. Modeling the evolution of continental subduction processes in the Pamir Hindu Kush region. Earth Planet Sci Lett, 2007, 259: 212–225
36 Li C, Hilst van der R D, Meltzer A S, et al. Subduction of the Indian lithosphere beneath the Tibetan plateau and Burma. Earth Planet Sci Lett, 2008, 274: 157–168
37 Hilst van der R D, Widiyantoro S, Engdahl E R. Evidence for deep mantle circulation from global tomography. Nature, 1997, 386: 578–584
38 Huang J, Zhao D. High-resolution mantle tomography of China and surrounding regions. J Geophys Res, 2006, 111: B09305, doi: 10.1029/2005JB004066
39 Zhao D P. Seismic images under 60 hotspots: Search for mantle plumes. Gondwana Res, 2007, 12: 335–355
40 Miller M S, Kennett B L N. Evolution of mantle structure beneath the northwest Pacific evidence from seismic tomography and paleogeographic reconstructions. Tectonics, 2006, 25: TC4002, doi: 10.1029/2005TC001909
41 Kim K H, Chiu J M, Pujol J, et al. Three-dimensional Vp and Vs structural models associated with the active subduction and collision tectonics in the Taiwan region. Geophys J Int, 2005, 162: 204–220, doi: 10.1111/j.1365-246X.2005.02657.x
42 Lallemand S, Font Y, Bijwaard H, et al. New insights on 3-D plates interaction near Taiwan from tomography and tectonic implications. Tectonophysics, 2001, 335: 229–253
43 Wang Y, Xu H Z. A study on convergence rate of the India plate to Eruasia subduction beneath Qinghai-Xizang Plateau—Inversion results from GPS observational data (in Chinese). Chin J Geophys, 2003, 46: 185–190
44 Sahu V K, Gahalaut V K, Rajput S, et al. Crustal deformation in the Indo-Burmese arc region: Implications from the Myanmar and Southeast Asia GPS measurements. Curr Sci, 2006, 90: 1688–1693
45 Zhao W J, Nelson K D, Project INDEPTH Team. Deep seismic reflection evidence for continental underthrusting beneath Southern Tibet (in Chinese). Acta Geoscint Sin, 1996, 17: 131–137
46 Zhao W J, Nelson K D, the Project INDEPTH Team. Deep seismic-reflection evidence for continental underthrusting beneath southern Tibet. Nature, 1993, 366: 557–559
47 Kosarev G, Kind R, Sobolev S V, et al. Seismic evidence for a detached Indian lithospheric mantle beneath Tibet. Science, 1999, 283: 1306–1309
48 Olsen K B, Stephenson W J, Geisselmeyer A. 3D crustal structure and long-period ground motions from a *M*9.0 megathrust earthquake in the Pacific Northwest region. J Seismol, 2008, 12: 145–159, doi: 10.1007/s10950-007-9082-y
49 Zang S X, Song H Z, Ning J Y. On the thermal structure of the Japan sea subduction zone and the effect of the heat sources (in Chinese). Acta Geophys Sin, 1993, 36: 164–173
50 Manning C E. The chemistry of subduction-zone fluids. Earth Planet Sci Lett, 2004, 223: 1–16
51 Holt W E, Ni J F, Wallace T C, et al. The active tectonics of the eastern Himalayan syntaxis and surrounding regions. J Geophys Res, 1991, 96: 14595–14632
52 Zhang J J, Ji J Q, Zhong D L, et al. Structural pattern of eastern Himalayan syntaxis in Namjagbarwa and its formation process. Sci China Ser D-Earth Sci, 2003, 47: 138–150
53 Santo T. On the characteristic seismicity in south Asia from Hindukush to Burma. Bull Inter Inst Seism Earth Eng, 1969, 6: 81–93
54 Fitch T J. Earthquake mechanisms in the Himalayan, Burmese, and Andaman regions and continental tectonics in Central Asia. J Geophys Res, 1970, 75: 2699–2709
55 Chandra U. Seismicity, earthquake mechanisms and tectonics of Burma, 20°–28°N. Geophys J Royal Astron Soc, 1975, 40: 367–381
56 Chandra U. Seismicity, earthquake mechanisms and tectonics along the Himalayan mountain range and vicinity. Phys Earth Planet Inter, 1978, 16: 109–131
57 Verma R K, Mukhopadhyay M, Ahluwalia M S. Seismicity, gravity and tectonics of northeast India and northern Burma. Bull Seism Soc Amer, 1976, 66: 1683–1694
58 Verma R K, Mukhopadhyay M, Nag A K. Seismicity and tectonics in south China and Burma. Tectonophysics, 1980, 64: 85–96
59 Liu J Z. The underthrust action of the Burma arc and seismogeological characters of Massif Chuan-Dian (in Chinese). Earthquake Res China, 1992, 8: 68–75
60 Steckler M S, Akhter S H, Seeber L. Collision of the Ganges-Brahmaputra Delta with the Burma Arc: Implications for earthquake hazard. Earth Planet Sci Lett, 2008, 273: 367–378
61 Khan P K. Variation in dip-angle of the Indian plate subducting beneath the Burma plate and its tectonic implications. Geosci J, 2005, 9: 227–234
62 Rangin C, Spakman W, Pubellier M, et al. Tomographic and geological constraints on subduction along the eastern Sundaland continental margin (South-East Asia). Bull Geol Soc France, 1999, 170: 775–788
63 Hu J F, Hu Y L, Xia J Y, et al. Crust-mantle velocity structure of S wave and dynamic process beneath Burma arc and its adjacent regions (in Chinese). Chin J Geophys, 2008, 51: 140–148
64 Li H J, Qin J Y. Earthquake mechanism and modern stress field in Burma arc and its adjacent area (in Chinese). Acta Seismol Sin, 1994, 16: 463–471
65 Angelier J, Baruah S. Seismotectonics in Northeast India: A stress analysis of focal mechanism solutions of earthquakes and its kinematic implications. Geophys J Int, 2009, 178: 303–326, doi: 10.1111/j.1365-246X.2009.04107.x
66 Engdahl E R, Hilst van der R D, Buland R. Global teleseismic earthquake relocation with improved travel times and procedures for depth determination. Bull Seism Soc Am, 1998, 88: 722–743

67 Engdahl E R, Villasefior A. Global Seismicity: 1900–1999. In: Lee W H K, Kanamori H, Jennings P C, et al., eds. International Handbook of Earthquake and Engineering Seismology. San Diego: Academic Press, 2002. 665–690
68 Hayes G P, Wald D J. Developing framework to constrain the geometry of the seismic rupture plane on subduction interfaces a priori—A probabilistic approach. Geophys J Int, 2009, 176: 951–964, doi: 10.1111/j.1365-246X.2008.04035.x
69 Hayes G P, Wald D J, Keranen K. Advancing techniques to constrain the geometry of the seismic rupture plane on the subduction interfaces a priori: Higher-order functional fits. Geochem Geophys Geosyst, 2010, 10: Q09006, doi: 10.1029/2009GC002633
70 Hayes G P, Wald D J, Johnson R L. Slab1.0: A three-dimensional model of global subduction zone geometries. J Geophys Res, 2012, 117: B01302, doi: 10.1029/2011JB008524
71 Zhang P Z, Deng Q D, Zhang G M, et al. Active tectonic blocks and strong earthquakes in the continent of China. Sci China Ser D-Earth Sci, 2003, 46(Suppl): 13–24
72 Wells D L, Coppersmith K L. New empirical relationships among magnitude, rupture width, rupture area, and surface displacement. Bull Seism Soc Am, 1994, 84: 974–1002
73 Bilham R, Gaur V K, Molnar P. Himalayan seismic harzard. Science, 2001, 293: 1442–1444
74 Bird P. An updated digital model of plate boundaries. Geochem Geophys Geosyst, 2003, 4: 1027, doi: 10.1029/2001GC00252
75 Guo S M, Xiang H F, Xu X W, et al. Characteristics and formation mechanism of the Longling-Lancang newly emerging fault zone in Quaternary in the southwest Yunnan (in Chinese). Seism Geol, 2000, 22: 277–284
76 Meade B J. Present-day kinematics at the India-Asia collision zone. Geology, 2007, 35: 81–84, doi: 10.1130/G22924A.1
77 Liu Z, Bird P. Kinematic modeling of neotectonics in the Persia-Tibet-Burma orogen. Geophys J Int, 2008, 172: 779–797
78 Copley A, McKenzie D. Models of crustal flow in the India-Asia collision zone. Geophys J Int, 2007, 169: 683–698
79 Copley A. Kinematics and dynamics of the southeastern margin of the Tibetan Plateau. Geophys J Int, 2008, 174: 1081–1100
80 Maurin T, Rangin C. Structure and kinematics of the Indo-Burmese Wedge: Recent and fast growth of the outer wedge. Tectonics, 2009, 28: TC2010, doi: 10.1029/2008TC002276